Effect of Arginine Loss in Myelin Basic Protein, as Occurs in Its Deiminated Charge Isoform, on Mediation of Actin Polymerization and Actin Binding to a Lipid Membrane in Vitro†

Joan M. Boggs,*,‡,§ Godha Rangaraj,‡ Christopher M. D. Hill,|| Ian R. Bates,||,⊥ Yew-Meng Heng,# and George Harauz||

Division of Structural Biology and Biochemistry, Research Institute, Hospital for Sick Children, 555 University Avenue, Toronto, ON, Canada M5G 1X8, Department of Laboratory Medicine and Pathobiology, University of Toronto, Toronto, ON, Canada M5G 1L5, Department of Paediatric Laboratory Medicine, Hospital for Sick Children, Toronto, ON, Canada M5G 1X8, and Department of Molecular and Cellular Biology, and Biophysics Interdepartmental Group, University of Guelph, 50 Stone Road East, Guelph, ON, Canada N1G 2W1

Received December 14, 2004

ABSTRACT: Myelin basic protein (MBP) binds to negatively charged lipids on the cytosolic surface of oligodendrocyte membranes and is most likely responsible for adhesion of these surfaces in the multilayered myelin sheath. It can also polymerize actin, bundle F-actin filaments, and bind actin filaments to lipid bilayers through electrostatic interactions. MBP consists of a number of posttranslationally modified isoforms of varying charge, including C8, in which six arginines are deiminated to the uncharged residue citrulline. The deiminated form decreases with development, but is increased in patients with the demyelinating disease multiple sclerosis. Here we investigate the effect of decreased net positive charge of MBP on its interaction with actin in vitro by comparing a recombinant murine form, rmC1, of the most highly charged unmodified isoform, C1, and a recombinant analogue of C8 in which six basic residues are converted to glutamine, rmC8. The dissociation constant of the less charged isoform rmC8 for actin was a little greater than that of rmC1, and rmC8 had somewhat reduced ability to polymerize actin and bundle F-actin filaments than rmC1. Moreover, rmC8 was more readily dissociated from actin by Ca^{2+}-calmodulin than rmC1, and the ability of the deiminated isoform to bind actin to lipid bilayers was reduced. These results indicate that electrostatic forces are the primary determinant of the interaction of MBP with actin. The spin labeled side chains of a series of rmC1 and rmC8 variants containing single Cys substitutions at seven sites throughout the sequence all became motionally restricted to a similar degree on binding F-actin, indicating that the entire sequence is involved in interacting with actin filaments or is otherwise structurally constrained in actin bundles. Thus, this posttranslational modification of MBP, which occurs early in life and is increased in multiple sclerosis, attenuates the ability of MBP to polymerize and bundle actin, and to bind it to a negatively charged membrane.

Myelin basic protein (MBP)[1] is 30% of the total protein and about 10% of the dry weight of myelin. It is bound to the cytosolic side of the oligodendrocyte (OL) membrane, primarily through electrostatic interactions with acidic lipids (reviewed in ref *1*). It is present throughout compact internodal myelin and is probably involved in adhesion of the cytosolic surfaces of the multilayered myelin sheath (*2*, *3*). Another function of MBP may be to interact with the cytoskeleton in oligodendrocytes, in cytosolic inclusions in myelin, and even in compact myelin, where MBP, actin, and tubulin occur in the radial component, a series of tight junctions that pass through many layers of myelin (*4*−*6*). MBP in solution binds to F-actin in a 1:1 mole ratio and induces the formation of ordered bundles of F-actin filaments (*7*). It also binds to G-actin in solution at an MBP/actin mole ratio of 1:2 and causes its polymerization into filaments under

† This work was supported by grants from the Canadian Institutes of Health Research to J.M.B. and G.H., from the Natural Sciences and Engineering Research Council to G.H., by a studentship from the Multiple Sclerosis Society of Canada to I.R.B., and by an Ontario Graduate Scholarship to C.M.D.H.

* To whom correspondence should be addressed. Mailing address: Division of Structural Biology and Biochemistry, Hospital for Sick Children, 555 University Ave., Toronto, ON, Canada M5G 1X8. Tel: (416)-813-5919. Fax: (416)-813-5022. E-mail: jmboggs@sickkids.ca.

‡ Division of Structural Biology and Biochemistry, Research Institute, Hospital for Sick Children.

§ University of Toronto.

|| University of Guelph.

⊥ Present address: Department of Physiology, McGill University, 3655 Promenade Sir William Osler, Montréal, Québec, Canada H3G 1Y6.

Department of Paediatric Laboratory Medicine, Hospital for Sick Children.

[1] Abbreviations: C1, naturally occurring, least modified, most positively charged isoform of 18.5 kDa MBP; C8, naturally occurring, least positively charged isoform of 18.5 kDa MBP with six Arg deiminated to Cit; CaM, calmodulin; Cit, citrulline; LUVs, large unilamellar vesicles; MARCKS, myristoylated alanine-rich C kinase substrate; MBP, myelin basic protein; MRP, MARCKS-related protein; OLs, oligodendrocytes; PC, phosphatidylcholine; PG, phosphatidylglycerol; SAILS, small angle integrated light scattering; rmC1, His-tagged recombinant form of murine C1; rmC8, His-tagged recombinant analogue of murine C8 with 6 Arg/Lys replaced by Gln.

10.1021/bi0473760 CCC: $30.25
Published on Web 02/11/2005

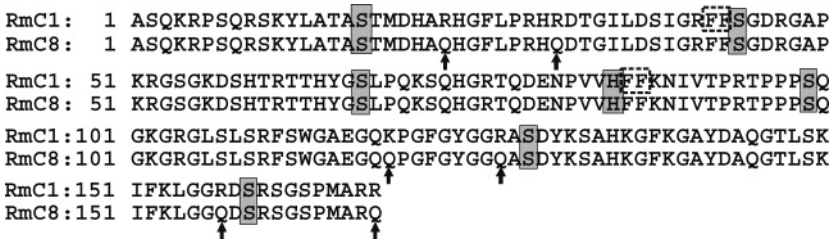

FIGURE 1: Amino acid sequences of rmC1 and rmC8, with residues that were mutated to Cys and spin-labeled indicated by gray boxes. The basic residues in rmC1 that were converted to Gln to yield rmC8 are indicated with an arrow. The LEH_6 tag was omitted for clarity. Adapted with permission from ref *26*.

otherwise nonpolymerizing low ionic strength conditions (*8*, *9*). The region 91−107 (murine sequence) near a triproline repeat has similarities to synapsin, also an actin-binding protein (*10*).

We showed earlier that MBP could bind actin filaments to the surface of negatively charged lipid vesicles, suggesting that it may be able to act as a membrane actin-binding protein (*11*). This property may allow it to transmit extracellular signals to the cytoskeleton (*12*). MBP also binds Ca^{2+}-calmodulin (CaM) (*13*−*15*), resulting in dissociation of MBP from actin bundles (*7*) and in depolymerization of actin filaments bound to MBP in solution (*8*). CaM-binding also causes dissociation of the MBP and the MBP-actin complex from lipid vesicles (*11*).

MBP (p*I* ∼10) may interact with anionic actin primarily through electrostatic interactions. The net positive charge of MBP is modified in vivo by a number of posttranslational modifications (*16*−*18*). The least modified, most highly charged 18.5 kDa isoform, C1, was used in our previous study. In the 18.5 kDa charge isoform called C8, six arginines are enzymatically deiminated to citrulline, decreasing its net positive charge from +19 to +13 at pH 7.4 (*19*). C8 is thus the least basic form of the protein. It has a diminished ability to cause adhesion of lipid bilayers and is dissociated from the lipid more easily than the 1east modified, most highly charged isoform, C1, by salt (*19*, *20*). The amount of C8 in myelin decreases during development but occurs in greater amounts in patients with the demyelinating disease multiple sclerosis (MS) (*19*, *21*).

Since naturally occurring C8 is scarce, we previously generated by site-directed mutagenesis a quasi-deiminated form of murine MBP called rmC8, which was designed to mimic the less cationic, natural form C8. It contains R/K→Q substitutions at the same deimination sites in human MBP that predominate in chronic MS, and it has properties similar to those of natural C8 (*22*). We produced and characterized a recombinant murine 18.5 kDa MBP (rmC1), which is unmodified posttranslationally (except for an LEH_6 tag) (*23*), for comparison with rmC8. The recombinant forms have been shown by experimental and modeling studies to be excellent analogues of the natural ones in most respects (*15*, *22*−*25*), and the recombinant forms are always comparable to each other.

The His tag should not be protonated at pH 8, as used in this study, and the net charge of rmC1 is +19, whereas that of rmC8 is +13, as for their natural counterparts. In the present study, we compare the abilities of rmC1 and rmC8 to polymerize actin and to bundle actin filaments. We examine the domains of MBP which interact with actin using rmC1 and rmC8 mutants with Cys substitutions at different sites for spin labeling (*26*). We also compare the abilities of native C1 and C8 to bind actin filaments to lipid bilayers.

MATERIALS AND METHODS

Proteins. The unmodified most highly charged recombinant Leu-Glu-His_6-tagged isoform of murine myelin basic protein (MBP), rmC1, was prepared as described (*23*). The quasi-deiminated mutant of murine MBP (rmC8) was generated from rmC1 by sequential site-directed mutations (first R25Q, then R33Q, K119Q, R127Q, R157Q, and finally R168Q, murine sequence numbering) using the QuikChange protocol (Stratagene, La Jolla, CA) as described previously (*22*). The sequences are shown in Figure 1. MBP is highly conserved between different species (*27*), although there is an R → K substitution at position 119 of murine MBP, one of the Arg deiminated in human C8. A series of matching Cys substitutions, S17C, S44C, S67C, H85C, S99C, S129C, and S159C, was generated in each of rmC1 and rmC8 (Figure 1) for the purpose of site-directed spin labeling by the sulfhydryl reactive spin label [1-oxyl-2,2,5,5-tetramethyl-D-pyrroline-3-methyl] methanethiosulfonate (MTS-SL) as described (*26*). MTS-SL was purchased from Toronto Research Chemicals (Toronto, ON). The recombinant proteins were purified by Ni^{2+}-NTA chromatography and dissolved in 10 mM Tris-HCl, pH 7.4, containing 10 mM NaCl. They were diluted with G or F buffer as required. The Ni^{2+}-NTA agarose beads were obtained from Qiagen (Mississauga, ON).

For certain experiments, the natural forms of MBP were used. The least modified, most highly positively charged 18.5 kDa isoform, C1, was purified from bovine brain MBP, and the most modified, least positively charged isoform, C8, was purified from human brain MBP as described (*18*, *28*, *29*). A murine recombinant form of the 21.5 kDa isoform of MBP was a kind gift from J. P. Mueller, Pfizer, Groton, CT (*30*). Egg L-α-phosphatidylcholine (PC) was purchased from Sigma (St. Louis, MO). L-α-Phosphatidylglycerol (PG; prepared from egg PC) was obtained from Avanti Polar Lipids, Inc. (Alabaster, AL). [^{3}H]-Cholesterol was from Amersham (Baie d'Urfe, QC, Canada).

G-actin and pyrene-labeled actin were purchased from Cytoskeleton (Denver, CO) and stored lyophilized at 4 °C. CaM was purchased from Calbiochem (San Diego, CA). Na_2ATP (grade 1) was purchased from Sigma (St. Louis, MO). Rabbit anti-actin antibody was purchased from Sigma (St. Louis, MO), rabbit polyclonal anti-MBP antibody (E5), IgG fraction, was a gift from Dr. E. Day (*31*), and goat anti-rabbit IgG conjugated to HRP was purchased from Jackson ImmunoResearch Labs (West Grove, PA). ECL Western blotting reagents were from Amersham.

Pyrene-Actin Polymerization. Actin polymerization was determined by monitoring the increase in fluorescence of pyrene-actin (*32*). A pyrene-actin solution was made in G buffer (5 mM Tris-HCl, pH 8.0, containing 0.2 mM Na_2ATP, 0.2 mM $CaCl_2$, 0.2 mM DTT, 0.001% TX-100) *(33)* at a concentration of 3 mg/8.1 mL G buffer and was left to stand at room temperature for 1 h. An aliquot was taken for protein assay, and the remainder was centrifuged at 100000*g* in a Ti 70.1 rotor for 1 h at 4 °C to remove any F-actin. Most of the supernatant was carefully removed, and an aliquot was taken for protein assay by the Bradford method (*34*). An aliquot (at least 275 μL) corresponding to 100 μg (2.3 nmol) actin was added to a 0.5 mL glass cuvette for each sample. Sufficient G buffer to give a total volume of 0.45 mL was added; the sample was excited at 365 nm, and emission measured at 407 nm for 5 min. For polymerization due to F buffer, a 50 μL aliquot of a 10 X solution of F buffer (0.5 M KCl, 20 mM $MgCl_2$, and 10 mM ATP in G buffer) was then added, the sample was mixed by inversion of the cuvette, and emission was measured for 30 min. For measurement of the dependence of polymerization on the amount of C1, rmC1, and rmC8 in G buffer, aliquots containing 100 μg actin (2.3 nmol) were added to test tubes, additional G buffer (to give a total volume of 0.45 mL after subsequent addition of the MBP solutions) was added to the actin, and baseline emission was read for 5 min. Aliquots of the MBP solutions were added to the G-actin in the test tubes, the samples were incubated for 45 min at room temperature, and emission was read for 3 min. A 50 μL aliquot of 10 X F buffer (5 mM Tris-HCl, pH 8 containing 2 mM $MgCl_2$, 50 mM KCl, 0.2 mM $CaCl_2$, 1 mM Na_2ATP, 0.5 mM DTT, 0.001% TX-100) was then added to each sample, the samples were incubated for 30 min at room temperature, and emission was read for 3 min. (The buffers contained 0.001% TX-100 to inhibit sticking of MBP to glass and plastic tubes as used by Vergères et al. (*35*) for the study of MARCKS-related protein (MRP) with actin.) Under similar conditions, at 4−25 °C, the critical concentration of muscle actin has been reported as 30 μg/mL (*36*). Dobrowolski et al. (*8*) determined that, in the presence of MBP, the critical actin concentration was close to zero.

An amount of rmC1 and rmC8, 19 μg (1.03 nmol), giving less than maximal polymerization was chosen for determination of the rate of polymerization of 100 μg (2.3 nmol) actin in the presence and absence of 0.15 M KCl, and for determination of the effect of CaM on the rate of depolymerization. For determination of the effect of 0.15 M KCl, aliquots of a 1.5 M KCl solution were added to the rmC1 and rmC8 solutions, such that the final concentration of KCl in the cuvette, after addition of the rmC1 and rmC8 solutions to the actin solution, would be 0.15 M. An aliquot containing 100 μg actin (2.3 nmol) was added to a cuvette with sufficient G buffer to give a total volume of 0.5 mL, after addition of the rmC1 or rmC8 solutions. The baseline emission of the G-actin solution was read for 5 min, and the rmC1 or rmC8 solution was added. The sample was mixed quickly by inversion, and emission was read every min until a steady state level was reached. For determination of the effect of CaM, the polymerization induced by rmC1 and rmC8 was measured similarly except that the total volume of the actin−rmC1/rmC8 solution was kept at 0.42 mL. After reaching a steady-state level, 30 μL of a CaM solution (1 mg/mL in G buffer) was added to the cuvette, the sample was mixed quickly by inversion, and emission was read until reaching a steady state. Then a 50 μL aliquot of 10 X F buffer was added, the sample was mixed by inversion, and emission was read until the value had plateaued again. The G and F buffers contained 0.2 mM $CaCl_2$; thus, the CaM was in the Ca^{2+}-bound form. The added mole ratio of actin/MBP/CaM was 2.2:1:1.7. At the end of the experiment, aliquots were lyophilized and the actin to MBP ratio in the samples was analyzed by slot blots.

Slot Blot Analysis. The lyophilized aliquots or pellets after sedimentation were dissolved in 2% SDS, incubated at 37 °C for 15 min, sonicated 2 min at 37 °C, and incubated again at 37 °C for 15 min. They were then diluted with Tris-buffered saline (TBS), and the actin to MBP ratio in the pellet was analyzed by slot blots by application of 100 μL of sample to a nitrocellulose membrane, presoaked in TBS, in a Bio-Dot SF microfiltration system with a 48-well slot format (Bio-Rad Laboratories, Inc., Hercules, CA). The dried membrane was blocked 1.5 h with 5% skim milk in TBS and incubated with anti-actin or anti-MBP Ab in 2.5% milk, followed by incubation with the HRP-conjugated anti-IgG. The membrane was exposed to ECL reagents. Spot densities were analyzed using a UVP image analyzer and compared to those of the standards in order to quantify the amount of each protein in the sample.

Turbidity Measurements. An increase in turbidity of the F-actin suspension due to bundling of actin filaments by rmC1 and rmC8 was measured from the light absorbance at 360 nm (Abs_{360}) as described (*8*). A stock solution of 1 mg/mL actin in G buffer was converted to F-actin in a 1.6 mL glass cuvette by addition of 100 μL of G-actin to 750 μL of F buffer. The sample was mixed by inversion, and Abs_{360} was read at intervals in a Hitachi U3210 spectrometer to establish a stable baseline reading. Aliquots of rmC1 or rmC8 solutions corresponding to 42 μg and sufficient F buffer to make the total volume 1 mL were added to the cuvette. The final concentration of actin was 100 μg/mL, and the mole ratio of actin to MBP was 1:1. The sample was rapidly mixed by inversion and Abs_{360} read immediately and at intervals (initially every minute) for 25−60 min.

Small Angle Integrated Light Scattering (SAILS). The bundling of F-actin by MBP was further monitored using a small angle integrated light scattering (SAILS) apparatus constructed in-house (*37*). The incident beam ($\lambda = 632.8$ nm) was produced by a 17 mW, vertically polarized, helium−neon continuous wave laser (Research Electro Optics Inc., Boulder, CO). Samples were loaded in a 3 × 3 mm quartz cuvette (Hellma Canada, Concord, ON, Canada) through which the beam was directed by a coated antireflection lens (Newport Corp., Mississauga, ON) positioned slightly in front of the laser. An iris diaphragm collimated the beam and prevented reflected light from contacting the sample. A diffusing plate (Oriel Corporation, Stratford, CT) was positioned 40 cm behind the sample to detect the scattered light. Two-dimensional images of the scattered light were taken by a charged couple device (CCD) camera (Princeton Instruments Inc., Trenton, NJ) with a wide-angle lens (Nikon, Japan), situated 53 cm behind the diffusing plate. The diffusing plate detected light scattered by 8.8−32.8° from the incident beam line. The software program WinView 1.2A (Princeton Instruments Inc., Trenton, NJ) was used to

collect and process images. Data were corrected for buffer scattering, refraction of the beam within the sample, and footprint effects on the diffusing screen. Scattering is represented as a function of the scattering vector q where $q = (4\pi n/\lambda)\sin(\theta/2)$. Here, $n = 1.33$, $\lambda = 632.8$ nm, and $\theta = 8.8-32.8°$.

F-actin was prepared by adding KCl and $MgCl_2$ from stock solutions to final concentrations of 50 mM and 2 mM, respectively, to G-actin in G buffer (final actin concentration 10 μM). This stock solution was used to make samples of 5 μM F-actin to which rmC1 or rmC8 was added to produce final molar ratios of 1:4 or 1:10 MBP/actin. These samples were incubated at room temperature for 1 h before data collection and were also allowed to reequilibrate for 5 min after transfer to the cuvette.

Electron Microscopy. Actin polymerized in F buffer, or actin-C1, actin-rmC1, and actin-rmC8 complexes in F buffer were used for electron microscopy without centrifugation. A 5 μL droplet of each sample was pipetted onto a Formvar-coated grid and negatively stained with 2% uranyl acetate. The samples were analyzed in a JEM 1230 transmission electron microscope (JEOL USA, Inc.) operated at 80 kV. Digital images of 1024 × 1024 pixels were acquired with a CCD camera (AMT Advantage HR camera system, AMT) attached to the microscope.

Actin-MBP Sedimentation Assay. The affinities of rmC1 and rmC8 for F-actin were measured using centrifugation conditions that pellet F-actin plus bound MBP but not free MBP. Aliquots of rmC1 and rmC8 corresponding to about 0.38 nmol of MBP were added to varying concentrations of actin from 0.16 to 4 μM in a total volume of 1 mL of F buffer in ultracentrifuge tubes. The samples were incubated at room temperature for 2 h. They were centrifuged at 100000*g* for 2 h at 4 °C in a Ti 70.1 rotor in a Beckman Optima L-90K ultracentrifuge. The supernatants were removed and the pellets were analyzed for MBP and actin by slot blots as described above. The concentrations of the rmC1 and rmC8 stock solutions were also checked by slot blots. The fractions of bound rmC1 and rmC8, F_b, were calculated and the data were fit to the function $A_t = MBP_t \times F_b + K_d \times F_b/(1 - F_b)$ according to Yarmola et al. (*38*), where MBP_t is the total rmC1 or rmC8 concentration and A_t is the total actin concentration. A similar experiment was carried out with C1, rmC1, and rmC8 using G buffer and 10 times higher MBP and actin concentrations.

EPR Spectroscopy. For addition to spin-labeled MBP samples, actin was dissolved in G buffer without DTT, containing 0.001% TX-100. Aliquots containing 130 μg of actin/200 μL were added to 50 μg/50 μL of each spin-labeled MBP sample in G buffer. The mole ratio of actin to MBP was 1.09:1. After 30 min at room temperature, 250 μL of 2X F buffer (without DTT) was added. The samples were mixed gently and incubated for 30 min at room temperature. They were centrifuged 15 min in an Eppendorf bench centrifuge at 9000*g*, the supernatant was removed, and the pellet was washed once with F buffer. The pellet containing the F-actin−MBP complex was loaded into a 50 μL capillary tube for EPR measurement. The EPR spectra were recorded in a Bruker ECS 106 spectrometer at room temperature using a microwave power of 10.0 mW, and a modulation amplitude of 1.0 G. The supernatant was assayed for protein and found to contain little protein, but had some detectable EPR signal.

Preparation of Large Unilamellar Vesicles. Aliquots of chloroform/methanol 2:1 solutions of the lipids were combined in the desired mole ratio. [^{3}H]-Cholesterol was added to give a specific activity of 100000 cpm/10 μmol of lipid. The solvent was evaporated under a stream of nitrogen with the tube maintained at room temperature in a water bath, and the lipid film was evacuated in a lyophilizer for 2 h. The dry lipid film was dissolved in 1−2 mL of benzene, frozen, and lyophilized overnight. The lipid (10−20 μmol) was hydrated in 500 μL of modified F buffer, with the divalent cations omitted. Multilamellar vesicles were prepared by freeze thawing five times using a dry ice/acetone bath followed by a 40 °C water bath and dispersing the lipid by vigorous vortex mixing. They were extruded through 0.1 μm pore filters to give large unilamellar vesicles (LUVs), as described (*20*). LUVs were diluted in modified F buffer to a final concentration of 1.5 mg or 1.95 μmol/100 μL.

Determination of Interaction of Actin and MBP Isoforms with LUVs. The natural C1, C8, and the recombinant 21.5 kDa isoforms of MBP were dissolved in modified G buffer at a concentration of 100 μg/100 μL. An amount of 100 μg (5.4 nmol) of MBP was added to 100 μL of LUVs in Eppendorf microcentrifuge tubes followed by an aliquot of G-actin solution containing 240 μg of G-actin (5.4 nmol). The sample was incubated at room temperature for 30 min to allow interaction of the proteins before addition of F buffer. Then sufficient F buffer (containing divalent cations; a minimum of 700 μL) was added to bring the total volume to 1.0 mL. The samples were mixed gently and incubated for an additional 30 min at room temperature.

The samples were centrifuged at 11800*g* for 15 min at 4 °C in an Eppendorf bench centrifuge. The supernatant was removed, and aliquots were taken for counting [^{3}H]-cholesterol, for protein assay, and for running on gels and/or slot blots. Aliquots for gel electrophoresis were lyophilized and taken up in NuPage sample buffer. The pellets were redispersed gently in 1 mL of F buffer and placed on a discontinuous sucrose density gradient in order to separate lipid-free actin−MBP complexes from lipid-bound MBP−actin complexes. The gradient was prepared by layering 1 mL each of 40% sucrose, 20% sucrose, 15% sucrose, and 10% sucrose, each made up in F buffer, in 5 mL Beckman Ultra-Clear ultracentrifuge tubes. The samples were centrifuged at 109000*g* for 18 h at 4 °C in a SW 55Ti rotor in a Beckman Optima L-90K ultracentrifuge. The lipid without protein sedimented in a hazy band on top of the 10% layer, whereas the lipid with protein sedimented as sharp bands which could be clearly seen by eye. The position and appearance of the band was noted, each sucrose layer was collected, and the bands were collected separately. After removal of most of the 40% layer, the bottom of the tube was washed out with 4.5 mL of F buffer to collect any pellet at the bottom, and transferred to 13.5 mL Nalgene polycarbonate (Ultrabottles) tubes. The bands were also transferred to 13.5 mL Nalgene polycarbonate tubes and diluted with 10 mL of F buffer. The tubes containing the washed out pellet from the bottom of the tube and the diluted band material were centrifuged at 85000*g* in a 70.1 Ti rotor for 1.5 h at 4 °C. The supernatant was removed, and aliquots were taken for [^{3}H] counting and protein assay. The pellet was redispersed in 0.5 mL of water, and aliquots were taken for counting, for protein assay, and for running on gels and/

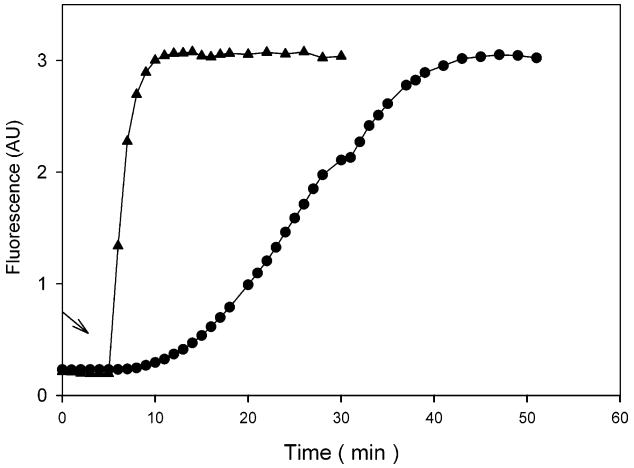

FIGURE 2: Time dependence of the increase in fluorescence in arbitrary units (AU) due to polymerization of pyrene-actin induced by F buffer (solid circles) and by recombinant rmC8 (solid triangles) in G buffer. F buffer or rmC8 was added at 5 min as indicated by the arrow.

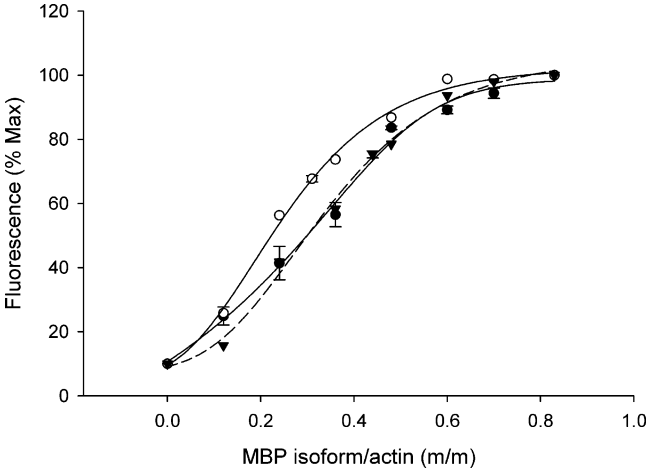

FIGURE 3: Dependence of increase in fluorescence (expressed as % of maximum value in each case), due to actin polymerization, on the mole ratio of MBP isoform to actin in G buffer, C1 (closed circles, solid line); rmC1 (open circles, solid line); and rmC8 (closed inverted triangles, dashed line). Each sample contained 2.3 nmol of pyrene-actin. Curves were fit to the data by nonlinear regression using a sigmoid 5-parameter equation by SigmaPlot. The average ± range from two experiments is shown for C1 and for one data point each for rmC1 and rmC8.

or slot blots. Aliquots of the sucrose layers without bands were counted for [^{3}H] and assayed for protein.

Protein was assayed by the Peterson method (*39*). Samples were run on NuPage 10% Bis-Tris gels (Novex, San Diego, CA) with known amounts of actin and MBP standards. Coomassie blue-stained gels were analyzed using a UVP image analyzer, and band areas were compared to those of the standards in order to quantitate the amount of each protein in the sample. An amount of 0.2 μg of each protein could be easily detected on the gels. Slot blots were carried out as described above.

RESULTS

Comparison of the Ability of C1, rmC1, and rmC8 To Cause Actin Polymerization and Filament Bundling. In addition to having a Leu-Glu-His_6 tag, rmC1 and rmC8 differ from native C1 and C8 in lacking two posttranslational modifications, an N-terminal acyl chain of 2−10 carbons in length, with 4−6 carbons predominating (*40*) and a mono- or dimethylated Arg 104 (murine sequence; human is Arg107, bovine is 106) (*41*). There are also some minor sequence differences between murine and bovine MBP with conserved replacements (*27*). However, the sequences of rmC1 and rmC8 are identical except for the replacement of 6 Arg(Lys) residues with Gln to mimic deimination of 6 Arg to Cit in human C8 (Figure 1), and thus can be used to determine the effect of a decrease in net positive charge by 6 on the ability of MBP to polymerize actin. In this paper, MBP is used as a general term for all isoforms of the protein, while C1, C8, rmC1, and rmC8 refer to specific natural and recombinant 18.5 kDa charge isoforms. The isoforms C1, rmC1, and rmC8 caused a rapid increase in fluorescence of pyrene-actin in G buffer (shown for rmC8 in Figure 2), indicating that they caused polymerization of actin. The fluorescence increase became nearly maximal at a mole ratio of each isoform to actin of about 0.5:1 (Figure 3), consistent with previous reports on a mixture of MBP charge isoforms (*7*, *8*), and equivalent to that induced by F buffer (containing 2 mM $MgCl_2$ and 50 mM KCl) (Figure 2). The rate of polymerization induced by MBP was faster than that induced by F buffer (Figure 2). Because MBP sticks to glass and plastic, the actin/MBP ratios of the combined solutions were checked by analysis on slot blots and confirmed to be identical for each isoform at each of the data points in Figure 3. The differences in the curves between rmC1 and C1 may be due to the contribution of the hexahistidine tag [CMD Hill et al., unpublished observations]. Generally, however, the recombinant rmC1 and natural C1 isoforms have behaved analogously in many studies, indicating that the former is a good mimic of the latter (*22*, *23*, *15*). The polymerization curves in Figure 3 for rmC1 and rmC8 can be compared, however, and show that, at low to intermediate molar ratios, the most highly charged isoform is somewhat more effective at polymerizing actin than the quasi-deiminated form.

Dobrowolski et al. (*8*) previously showed that Ca^{2+}-CaM caused depolymerization of actin polymerized by a mixture of MBP isoforms. Thus, we compared the rates of Ca^{2+}-CaM-induced depolymerization of actin polymerized by rmC1 and rmC8. Ca^{2+}-CaM caused depolymerization of actin in the presence of rmC8 (Figure 4B) noticeably faster than in the presence of rmC1 (Figure 4A), indicating that it caused dissociation of rmC8 from actin more readily than the more positively charged rmC1. The initial rate of Ca^{2+}-CaM-mediated depolymerization in the presence of rmC8 was two times greater than in the presence of rmC1 (Table 1). The addition of F buffer after Ca^{2+}-CaM-induced depolymerization caused repolymerization to similar extents for both rmC1 and rmC8 samples, indicating that CaM was not interfering directly with polymerization.

An increase in ionic strength should inhibit the electrostatic interaction between MBP and actin and decrease the rate of polymerization. The presence of 0.15 M KCl significantly slowed the rate of polymerization induced by both isoforms. This allowed comparison of the rate of polymerization by rmC1 and rmC8 under these conditions. Both isoforms induced polymerization at a similar rate (Figure 4C,D, respectively, Table 1). Measurement of the turbidity of the actin−MBP solutions from the absorbance at 360 nm (not shown) suggested that both rmC1 and rmC8 caused bundling

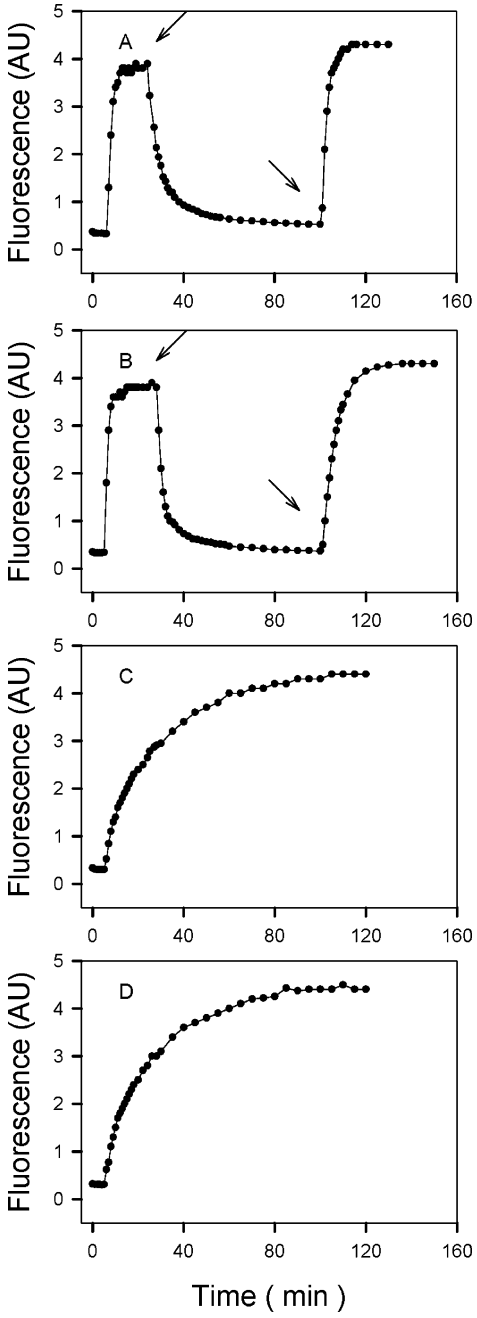

FIGURE 4: (A, B) Time dependence of the increase in fluorescence in arbitrary units (AU) due to polymerization of 2.3 nmol of pyrene-actin induced by 1 nmol of MBP isoform and decrease in fluorescence due to depolymerization following dissociation of MBP isoform by 1.8 nmol of CaM for (A) rmC1 and (B) rmC8. CaM was added at the plateau at the time indicated by the first arrow. F buffer was added at the time indicated by the second arrow. (C, D) Time dependence of the increase in fluorescence due to polymerization of 2.3 nmol of pyrene-actin induced by 1 nmol of MBP isoform in the presence of 0.15 M KCl for (C) rmC1 and (D) rmC8. In all cases, rmC1 and rmC8 were added at the point of sharp increase in fluorescence at around 5 min.

of actin filaments, as found by Barylko and Dobrowolski (*7*) using a mixture of MBP isoforms. This idea was confirmed by electron microscopy using equimolar ratios of MBP to actin (Figure 5). The bundles in the presence of rmC1 and rmC8 appear similar to those caused by C1 (not shown for C1) and by a mixture of MBP isoforms reported previously (*7*). They were generally 30−45 nm in diameter,

Table 1: Rate of Actin Polymerization and CaM-Mediated Depolymerization in the Presence of rmCl Relative to rmC8[a]

	rate[b]		rate ratio	
	rmC1	rmC8	rmC1/rmC8	*n*
actin depolymerization in presence of CaM	4.1 ± 0.4	8.8 ± 0.02	0.54 ± 0.08	2
actin polymerization in G buffer + 0.15 M KCl	2.5 ± 0.1	2.4 ± 0.1	1.02 ± 0.06	3

[a] Absolute rates varied from one experiment to another depending on the batch of pyrene-actin. However, the relative differences between rmC1 and rmC8 were similar in different experiments. Therefore, the rates from a representative experiment are shown and ratios of the rate of rmCl-induced depolymerization or polymerization to that of rmC8 from *n* different experiments were averaged to give the mean rate ratios shown, ± standard deviation ($n = 3$) or range ($n = 2$). [b] Rate in fluorescence units/min for a representative experiment determined by fit of the first 3−4 data points to a straight line using SigmaPlot. Slope ± standard error of the linear regression is shown.

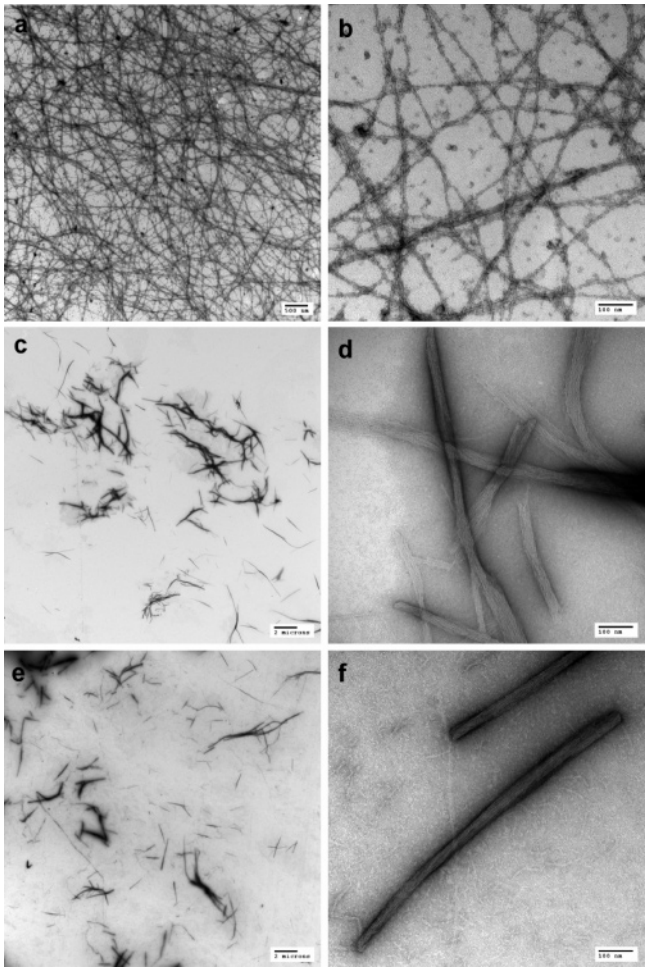

FIGURE 5: Electron micrographs of (a) F-actin obtained by polymerization of G-actin in F buffer; (b) F-actin at higher magnification; (c) F-actin in the presence of equimolar rmC1 in F buffer; (d) F-actin in the presence of equimolar rmC1 in F buffer, higher magnification; (e) F-actin in the presence of equimolar rmC8 in F buffer at low magnification; (f) F-actin in the presence of equimolar rmC8 in F buffer, higher magnification. Bar indicates 500 nm (a), 2 μm (c, e), 100 nm (b, d, f).

whereas undecorated F-actin filaments were 6−7.5 nm in diameter.

Small angle integrated light scattering (SAILS) was used to quantify the extent of actin bundling effected by rmC1 and rmC8. This method has the advantage that it requires

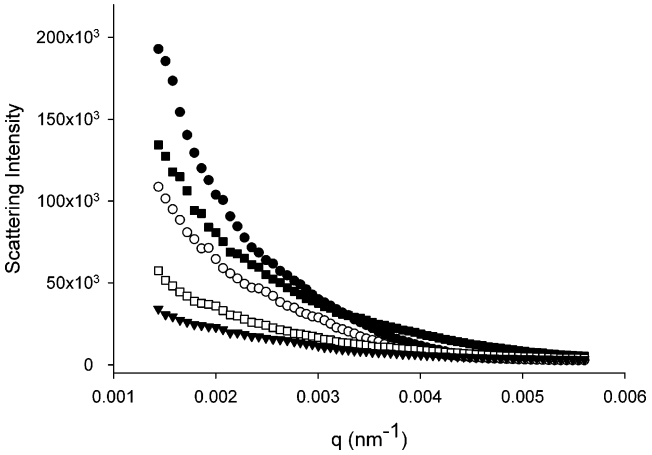

FIGURE 6: Small angle integrated light scattering (SAILS) assay of the actin-bundling activity of rmC1 (circles) and rmC8 (squares). MBP was added to solutions of 5 μM F-actin to final molar ratios of 1:10 (open symbols) and 1:4 (closed symbols) MBP:actin, and the sample was allowed to equilibrate for 1 h prior to data collection. Scattering due to F-actin alone is shown for comparison (triangles). Data are represented as a function of q, where q is equal to the magnitude of the momentum transfer vector and $q = (4\pi n/\lambda) \sin(\theta/2)$. These q values correspond to scattering angles (θ) of 8.8−32.8°.

no dyes, labels, or fixatives and provides a global picture of sample properties, rather than the localized information obtainable by EM. Scattering from solutions of either G-actin or MBP alone (not shown) did not display q-dependent scattering as expected, as the length scales probed in this experiment ($2\pi/q$) were much larger than MBP or actin monomers. Polymerized actin exhibited q-dependent scattering (Figure 6), as expected, as the filament length should exceed the minimum observable length scales. The addition of rmC1 or rmC8 to F-actin resulted in increased light scattering (Figure 6). Light scattering induced by rmC1 was greater than that induced by the less cationic rmC8 at MBP/actin ratios of 1:10 and 1:4 although the difference appeared to be more marked at a 1:10 ratio.

Actin−MBP Binding Assay. Representative equilibrium binding curves from a sedimentation assay of rmC1 and rmC8 with F-actin are shown in Figure 7. The dissociation constants for rmC1 and rmC8 were 36.3 nM and 44.5 nM, respectively. In a separate experiment using G-actin, the natural isoform C1 was included for comparison with the recombinant ones. C1 and qC1 bound with dissociation constants of 32.9 nM and 33.2 nM, respectively. However, this assay requires that the MBP also polymerize and bundle the G-actin so that the complex sediments. The rmC8 and actin did not sediment at all actin/rmC8 ratios, probably due to the decreased ability of rmC8 to bundle actin. Thus, its dissociation constant could not be measured by this method when using G-actin.

Interaction of Actin with Different Regions of rmC1 and rmC8. Although MBP was shown to bind to F-actin in a 1:1 mole ratio, it caused the maximum increase in pyrene-actin fluorescence at an MBP:actin mole ratio of 0.5:1, suggesting that one molecule of MBP has two binding sites for actin (*7*, *8* and Figure 3). Proteolytic fragments of MBP from the N-terminal half and the C-terminal half both bound to actin (*8*, *9*). To determine more precisely which regions of MBP bind to actin, we investigated the effect of F-actin binding on the EPR spectrum of rmC1 and rmC8 spin labeled at

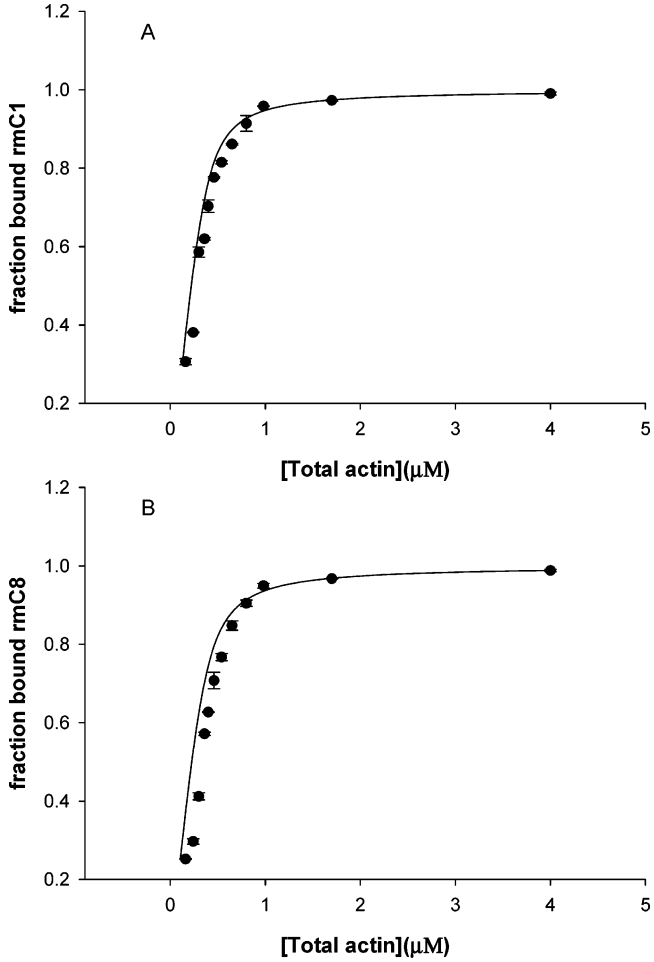

FIGURE 7: Binding of rmC1 (A) and rmC8 (B) to F-actin determined from a sedimentation assay. Average ± range from an experiment assayed in duplicate is shown. Data were fit assuming a single binding site to the function given in Materials and Methods. The fit yielded a k_d of 36.3 nM ($R = 0.997$) for rmC1 and 44.5 nM ($R = 0.995$) for rmC8.

different sites using variants with Cys substitutions. The spectrum shown in Figure 8B contains a minor sharp component resembling that of spin-labeled MBP in solution (Figure 8A), and a major broad component with large hyperfine splitting (indicated by an arrow in Figure 8B). The immobilized component is due to a larger population of the spin-labeled MBP whose spin-labeled side chain is in contact with, and probably trapped between, actin monomers in actin filaments or between actin filaments in the actin bundles. The mobile component reflects a smaller population, which is most likely unbound spin-labeled MBP. There was little protein in the supernatant by a protein assay, but there was some EPR signal. Washing the pellet did not remove it completely (Figure 8C), suggesting that it is due to unbound spin-labeled MBP in equilibrium with bound spin-labeled MBP. The separation of the low-field broad peak from the center peak was 28−29 G for all spin-labeled Cys at residues 17, 44, 67, 85, 99, 129, and 159 in both rmC1 and rmC8 on binding to F-actin. This hyperfine splitting value increases with decrease in mobility. Its similar value for all variants indicates a similar degree of immobilization for all residues, despite the fact that some of them in rmC8 (129 and 159) are each separated from an R → Q substitution by only one residue. In contrast, there was more variation in the degree of motional restriction when rmC1 and rmC8 spin-labeled

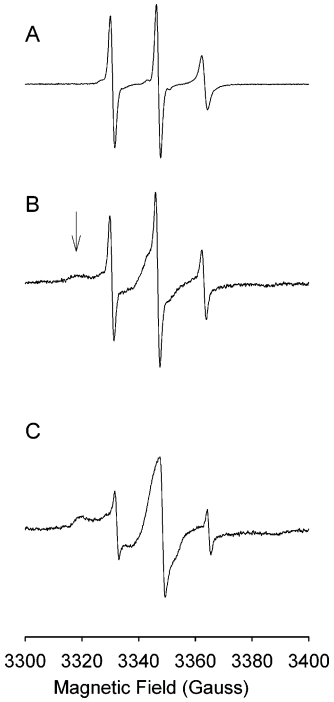

FIGURE 8: EPR spectra of spin-labeled rmC1−C85 (A) in F buffer and (B) bound to an equimolar amount of F-actin in F buffer (pellet before washing), and (C) pellet after washing with F buffer. The spectrum in part A is characteristic of rapid isotropic motion. All of the spin-labeled MBPs in F buffer gave spectra virtually identical to that in part A and similar to those in parts B and C when bound to F-actin. F-actin caused motional restriction of the spin labeled side chain of MBP resulting in the broad spectral component whose low-field peak is indicated by an arrow in part B. The sharp spectral component is due to unbound spin-labeled rmC1 and can be partly removed by washing, giving the spectrum shown in part C. The fraction of spin label giving rise to the broad spectral component in parts B and C is significantly greater than that giving rise to the sharp component, since the area of the peak is proportional to the amount of spin label contributing to the peak. Since the high-field broad peak was of lower intensity, the hyperfine splitting values were obtained from spectra of washed pellets, such as that shown in part C, by measuring the separation of the broad low-field peak (at the point of maxium intensity) from the center peak at the point where it crosses the baseline. These hyperfine splitting values were 28−29 G for all spin-labeled residues in rmC1 and rmC8, indicating significant motional restriction of all of the spin-labeled side chains.

on different residues were bound to lipid vesicles or to CaM (*26*, *24*). This supports the conclusion that the immobilization of spin-labeled residues by F-actin is due to restriction of MBP side chain motion within the bundles.

Comparison of the Ability of C8 and C1 To Bind Actin to LUVs. Our earlier sedimentation analysis (*11*) showed that C1 bound to PC/PG 4:1 (mol/mol) large unilamellar lipid vesicles (LUVs) binds F-actin bundles to the surface of the LUVs. To determine if a decrease in the net positive charge of C1 decreases its ability to bind actin to negatively charged PC/PG 4:1 LUVs, the naturally occurring, less charged deiminated C8 form of MBP was compared to the C1 form. The interaction of actin with membrane-bound C1 and C8 was determined from cosedimentation of actin and C1/C8 with the LUVs. The samples were first centrifuged for 15 min at 11800*g*, a low speed at which uncomplexed MBP, G-actin, and F-actin did not sediment and could thus be separated from the MBP−F-actin complex and protein-bound LUVs (*11*). The latter can be sedimented at this low speed in the high-salt F buffer used (*11*). The total amount of protein remaining in the supernatant was determined by a protein assay, and the relative amounts of MBP and actin were determined by separation on gels and comparison of band densities with standards as reported previously (*11*), as well as by slot blots. The pellets were then resuspended in F buffer and ultracentrifuged at high speed (109000*g*) on a discontinuous sucrose gradient in order to separate any actin−MBP complex unbound to lipid from a lipid-bound MBP−actin complex and MBP−lipid or protein-free lipid vesicles. Bands and different sucrose layers were collected and the amounts of lipid, actin, and MBP in each were determined.

Table 2: Actin and MBP Isoforms Associated with Lipid Vesicles[a]

MBP isoform	% added MBP bound to lipid vesicles: no actin	% added MBP bound to lipid vesicles: with actin	% added actin in supernatant[b]	% added protein at bottom of sucrose density gradient[c]: actin	% added protein at bottom of sucrose density gradient[c]: MBP	actin/MBP (m/m) bound to lipid vesicles[c,d]
18.5 kDa C1	95	100	27	0	0	0.8, 0.9
18.5 kDa C8	91	95	16	13	5	0.4
21.5 kDa MBP	95	100	47	0	0	0.7

[a] PC/PG 4:1 (m/m) LUVs. Initial mole ratio of actin/MBP isoform was 1:1. [b] After low-speed centrifugation in an Eppendorf centrifuge. [c] After high-speed ultracentrifugation of the low-speed pellet on a sucrose density gradient. [d] Two lipid protein bands were recovered from the sucrose density gradient partway into the 10% layer and on top of the 15% layer for C1. One band was recovered for C8 and the 21.5 kDa isoform halfway into the 10% layer in each case.

In the absence of actin, most of the C1 and C8 were bound to the LUVs (Table 2). In the presence of actin, none of the C1 or C8 was found in the supernatant, but further analysis showed that although all of the C1 was bound to LUVs, not all of the C8 was bound to LUVs. In the presence of C1, 27% of the actin remained in the supernatant (Table 2). Ultracentrifugation of the pellet on a sucrose density gradient showed that the actin−C1 complex was bound to the LUVs in two opaque lipid−protein bands partway into the 10% sucrose layer and on top of the 15% sucrose layer. In the absence of MBP, actin does not sediment with the lipid vesicles (*11*). Thus, actin is bound to the lipid-bound C1. Although the lipid/protein ratio of the two bands differed, quantification of the actin and C1 in the bands by densitometry of Coomassie blue-stained gels or by slot blots indicated a similar actin/C1 mole ratio, 0.8:1 in the lower density band and 0.9:1 in the higher density band, close to the starting ratio of 1:1 (Table 2). No protein was found at the bottom of the tube, indicating that there was no actin−C1 complex not bound to lipid. The actin−C1 complex in the absence of LUVs sediments to the bottom of the tube and can be seen as a pellet; 100% of the added protein is recovered in this pellet (*11*).

In the presence of C8, although only 16% actin remained in the supernatant, another 13% was found at the bottom of the sucrose density gradient complexed to a small amount of C8 (Table 2). An opaque lipid−protein band which sedimented halfway into the 10% sucrose layer contained 84% of the added C8 and 30% of the actin. The remaining actin may have been distributed throughout the gradient due to dissociation during centrifugation. The actin/C8 mole ratio in the protein−LUVs complex was 0.4:1, significantly less than the starting ratio. Thus, C8 could also bind F-actin to LUVs, but not as much as C1 did. Actin binding caused

dissociation of some C8 from the LUVs resulting in some lipid-free C8−actin complex. This dissociation did not occur for C1, even for LUVs containing only 10% acidic lipid, which bind less C1 than LUVs containing 15% or more acidic lipid (*11*).

Contribution of Exon II in 21.5 kDa Isoform of MBP to Actin Binding. MBP also occurs as size isoforms from 14 to 21.5 kDa. The 21.5 kDa isoform contains an additional peptide segment encoded by exon II, which is absent in the 18.5 kDa form. Since there is some similarity between the exon II segment (59−84) of the 21.5 kDa isoform of MBP and the actin-binding protein synapsin (*10*), in addition to that in the 91−107 triproline region (120−136 of 21.5 kDa sequence), we also determined the ability of recombinant 21.5 kDa MBP to bind actin to LUVs. The domain encoded by exon II has a greater linear positive charge density than the rest of the protein. However, its binding of actin to the LUVs was similar to or a little less than that of 18.5 kDa C1. In the single lipid−protein band recovered from the bottom of the 10% sucrose level of the sucrose density gradient, the actin/MBP mole ratio was 0.7:1 (Table 2). The unbound actin was found in the low-speed supernatant, and there was no protein at the bottom of the gradient. In a separate study, the 21.5 kDa isoform has been found to polymerize and bundle actin somewhat less efficiently than the 18.5 kDa isoform (rmC1) (*42*).

DISCUSSION

MBP binds to G-actin and causes its polymerization, and it bundles actin filaments (*7*, *8*). Other highly basic polycationic proteins such as histone, polyamines, fesselin, and calponin (*43*−*46*) and peptides such as the basic effector domain of MRP, similar to that of MARCKS, also increase the rate of polymerization of actin and bundle actin filaments (*38*, *47*, *48*), indicating that electrostatic interactions are a major determinant of actin polymerization and bundling activity. Therefore, it was expected that a less charged isoform of MBP might not bind, polymerize, and bundle actin as well as the most positively charged isoform. Inhibition of polymerization by rmC1 and rmC8 in the presence of 0.15 M KCl confirmed that electrostatic interactions contribute to actin binding by MBP. Furthermore, CaM caused more rapid dissociation of rmC8 from actin than rmC1. CaM has been found to bind to both rmC1 and rmC8 in a Ca^{2+}-dependent way and with similar or slightly diminished affinity for rmC8 relative to rmC1; however, rmC1 has only one CaM binding site whereas rmC8 may have an additional site (*15*, *49*). Thus, the greater ability of CaM to cause dissociation of rmC8 may be due to greater binding or greater accessibility of a binding site of rmC8 to CaM, or to the lower affinity of rmC8 for actin.

In experiments with lipid-bound actin and natural MBP charge isoforms, C8 also did not bind actin filaments to lipid bilayers as well as C1. This could be partly due to a lower affinity of C8 for the lipid than C1, since some C8 also dissociated with the actin, and partly due to a higher net negative surface charge of the bilayer in the presence of C8, which repels the actin under conditions where the actin remains bound to lipid-bound C1. In the case of the MARCKS effector domain, theoretical calculations showed that the electrostatic potential was quite positive above the peptide, even when bound to acidic lipids (*50*). A similar effect for MBP would allow it to bind actin while simultaneously binding to the lipid negative surface charge. However, an increase in the net negative surface charge of the lipid bilayer due to an increase in the ratio of negatively charged to neutral lipid (*11*) repels actin, but C1 remains bound to the lipid. Reduction of the net positive charge of C8 would also increase the net negative surface charge of the C8-lipid bilayer and repel actin. Thus, the reduction of net positive charge of C8 reduces its ability to bind simultaneously to negatively charged lipid and negatively charged actin.

However, despite its reduction in net charge by 6, rmC8 was still able to polymerize and bundle actin and to bind it to lipid vesicles, although it was somewhat less efficient in these functions than rmC1, particularly at low rmC8 to actin ratios. This may be due to its greater dissociation constant for actin. The rates of polymerization by rmC1 and rmC8 in the presence of 0.15 M KCl were similar. At a roughly equimolar ratio of actin to MBP, electron microscopy indicated that actin bundles of similar structure were induced by both rmC1 and rmC8, and spin-labeled residues on rmC8, lacking 6 basic residues, were immobilized similarly to those in rmC1. The domain of 21.5 kDa MBP encoded by exon II, which also has similarities to synapsin and has a higher linear charge density than the rest of the protein, does not seem to contribute to actin binding, since the exon II^+ 21.5 kDa isoform of MBP bound actin to the lipid bilayer less well than the 18.5 kDa form lacking this exon II-encoded sequence. It also polymerized and bundled actin somewhat less efficiently than the 18.5 kDa isoform (*42*). The comparable rate of polymerization induced by rmC8 and similar degree of interaction of actin with spin-labeled residues of rmC8 despite its reduced electrostatic interactions suggests that hydrophobic and/or hydrogen bonding interactions may also contribute to actin binding by MBP. Phenylalanyl residues in the MARCKS/MRP effector domain were found to contribute to its actin-binding affinity (*38*) and rate of F-actin nucleation (*47*), and MBP contains two sets of Phe-Phe pairs at positions 42−43 and 86−87 (murine sequence numbering, Figure 1).

Earlier studies indicated that MBP had two actin-binding sites, one in the N-terminal and another in the C-terminal portion (*9*). However, we show that spin labels bound to Cys at different positions throughout the sequence of rmC1 and rmC8 were immobilized to a similar extent by actin binding. This result suggests that the entire molecule is involved in binding to two actin monomers or cross-linking actin filaments, and thus is structurally constrained, in contrast to its flexibility in solution. Basic residues are distributed throughout the sequence and may serve to anchor the entire molecule to actin. MBP is an intrinsically unstructured protein (*51*−*54*), similar to MARCKS and other regulatory proteins in cells, giving it sufficient flexibility to bind to a charged surface over its entire length and to acquire whatever local conformation is necessary to optimize binding to several different targets. Unlike MBP, however, intact MARCKS does not bind to G-actin or induce polymerization of actin although it binds to F-actin and bundles actin filaments (*55*), whereas intact MRP did not cause bundling although it binds to F-actin (*56*). This difference in behavior of the intact proteins from the effector domain is probably

due to the fact that the sequence of MRP and MARCKS outside the effector domain is highly acidic.

Jones et al. (*57*) have pointed out that the interaction of proteins with polyanions such as actin is characterized by a lower degree of specificity, albeit high affinity, than for other intermolecular interactions. These interactions may nevertheless be functional. Polycationic proteins such as MBP can interact with a number of polyanionic proteins and surfaces such as cytosolic membrane phospholipids, actin, microtubules, and polynucleotides. Myelin basic protein can also bind to microtubules in vitro (*58*). Isoforms of MBP containing the segment encoded by exon II have been found to also localize in the nucleus, where they may bind to polynucleotides, whereas the isoforms lacking this segment mainly bind to the cytosolic surface of the membrane (*59*). Such a variety of interactions may play a physiological role, especially for a protein as abundant in OLs and myelin as MBP.

Colocalization studies by immunohistochemistry in immature cultured oligodendrocytes (OLs) indicate that MBP is closely associated with microtubules and actin microfilaments (*60*). MBP might also bind actin to microtubules. In *Shiverer* mouse OLs which lack MBP, actin microfilaments are not colocalized with microtubular structures as they are in the wild-type OLs (*61*). Since MBP can bind actin to the lipid bilayer, it may also be able to bind F-actin to the cytosolic side of the plasma membrane of the oligodendrocyte or to the cytosolic side of myelin. The radial component found in compact myelin contains tubulin, actin, MBP, CNPase, and glycosphingolipids (*4*−*6*). Although the primary function of MBP seems to be to cause adhesion between the cytosolic surfaces of myelin, it may have other functions as well. Indeed, many cytoskeletal proteins are multifunctional (*62*). MBP may also play a role in signaling in oligodendrocytes and myelin. Anti-galactosylceramide antibody mediates signals which cause depolymerization of the cytoskeleton and other signal transduction events in cultured OLs. MBP is required for these effects, suggesting that it is involved in transduction of the signal (*12*).

CONCLUSIONS

The results presented here show that deimination of MBP, which occurs during development or in MS, could modulate this protein's ability to polymerize actin and to bind it to the lipid bilayer, and increase its susceptibility to CaM-mediated dissociation from actin. Ongoing studies in our laboratory with phosphorylated MBP indicate that this posttranslational modification has a similar effect (*63*), and a synergy between several different kinds of posttranslational modifications, as well as lipid- and CaM-binding, might be operative in vivo.

ACKNOWLEDGMENT

The authors are grateful to Ms. Lisa Hewer and Dr. Ross Hallett for assistance with the light scattering experiments.

REFERENCES

1. Boggs, J. M., Moscarello, M. A., and Papahadjopoulos, D. (1982) Structural organization of myelin. Role of lipid-protein interactions determined in model systems, in *Lipid-Protein Interactions* (Jost, P., Griffith, O. H., Eds.) Vol. 2, pp 1−51, John Wiley and Sons, New York.
2. Omlin, F. X., Webster, H. D., Palkovits, C. G., and Cohen, S. R. (1982) Immunocytochemical localization of basic protein in major dense line regions of central and peripheral myelin, *J. Cell Biol. 95*, 242−248.
3. Readhead, C., Takasashi, N., Shine, H. D., Saavedra, R., Sidman, R., and Hood, L. (1990) Role of myelin basic protein in the formation of central nervous system myelin, *Ann. N.Y. Acad. Sci. 605*, 280−285.
4. Karthigasan, J., Kosaras, B., Nguyen, J., and Kirschner, D. A. (1994) Protein and lipid composition of radial component-enriched CNS myelin, *J. Neurochem. 62*, 1203−1213.
5. Pereyra, P. M., Horvath, E., and Braun, P. E. (1988) Triton X-100 extractions of central nervous system myelin indicate a possible role for the minor myelin proteins in the stability in lamellae, *Neurochem. Res. 13*, 583−595.
6. Gillespie, C. S., Wilson, R., Davidson, A., and Brophy, P. J. (1989) Characterization of a cytoskeletal matrix associated with myelin from rat brain, *Biochem. J. 260*, 689−696.
7. Barylko, B., and Dobrowolski, Z. (1984) Ca^{2+}-calmodulin-dependent regulation of F-actin-myelin basic protein interaction, *Eur. J. Cell Biol. 35*, 327−335.
8. Dobrowolski, Z., Osinska, H., Mossakowska, M., and Barylko, B. (1986) Ca^{2+}-calmodulin-dependent polymerization of actin by myelin basic protein, *Eur. J. Cell Biol. 42*, 17−26.
9. Roth, G. A., Gonzalez, M. D., Monferran, C. G., De Santis, M. L., and Cumar, F. A. (1993) Myelin basic protein domains involved in the interaction with actin, *Neurochem. Int. 23*, 459−65.
10. Pedraza, L. T., Roth, G. A., and Cumar, F. A. (1988) Identification as synapsin of a synaptosomal protein immunoreacting with anti-myelin basic protein antiserum, *J. Neurochem. 51*, 413−420.
11. Boggs, J. M. and Rangaraj, G. (2000) Interaction of lipid-bound myelin basic protein with actin filaments and calmodulin, *Biochemistry 39*, 7799−7806.
12. Dyer, C. A., Philibotte, T. M., Wolf, M. K., and Billings-Gagliardi, S. (1994) Myelin basic protein mediates extracellular signals that regulate microtubule stability in oligodendrocyte membrane sheets, *J. Neurosci. Res. 39*, 97−107.
13. Grand, R. J. A., and Perry, S. V. (1980) The binding of calmodulin to myelin basic protein and histone H2B, *Biochem. J. 189*, 227−240.
14. Chan, K.-F. J., Robb, N. D., and Chen, W. H. (1990) Myelin basic protein: interaction with calmodulin and gangliosides, *J. Neurosci. Res. 25*, 535−544.
15. Libich, D. S., Hill, C. M. D., Bates, I. R., Hallett, F. R., Armstrong, S., Siemiarczuk, A., and Harauz, G. (2003) Interaction of the 18.5 kDa isoform of myelin basic protein with Ca^{2+}-calmodulin: effects of deimination assessed by intrinsic Trp fluorescence spectroscopy, dynamic light scattering, and circular dichroism, *Protein Sci. 12*, 1507−1521.
16. Zand, R., Li, M. X., Jin, X., and Lubman, D. (1998) Determination of the sites of posttranslational modifications in the charge isomers of bovine myelin basic protein by capillary electrophoresis-mass spectroscopy, *Biochemistry 37*, 2441−2449.
17. Deibler, G. E. and Martenson, R. E. (1973) Chromatographic fractionation of myelin basic protein. Partial characterization and methylarginine contents of the multiple forms, *J. Biol. Chem. 248*, 2392−2396.
18. Chou, F. C.-H., Chou, C.-H. J., Shapira, R., and Kibler, R. F. (1976) Basis of microheterogeneity of myelin basic protein, *J. Biol. Chem. 251*, 2671−2679.
19. Wood, D. D. and Moscarello, M. A. (1989) The isolation, characterization, and lipid-aggregating properties of a citrulline containing myelin basic protein, *J. Biol. Chem. 264*, 5121−5127.
20. Boggs, J. M., Yip, P. M., Rangaraj, G., and Jo, E. (1997) Effect of posttranslational modifications to myelin basic protein on its ability to aggregate acidic lipid vesicles, *Biochemistry 36*, 5065−5071.
21. Moscarello, M. A., Wood, D. D., Ackerley, C., and Boulias, C. (1994) Myelin in multiple sclerosis is developmentally immature, *J. Clin. Invest 94*, 146−154.
22. Bates, I. R., Libich, D. S., Wood, D. D., Moscarello, M. A., and Harauz, G. (2002) An Arg/Lys→Gln mutant of recombinant murine myelin basic protein as a mimic of the deiminated form implicated in multiple sclerosis, *Protein Expression Purif. 25*, 330−341.
23. Bates, I. R., Matharu, P., Ishiyama, N., Rochon, D., Wood, D. D., Polverini, E., Moscarello, M. A., Viner, N. J., and Harauz, G.

(2000) Characterization of a recombinant murine 18.5-kDa myelin basic protein, *Protein Expression Purif. 20*, 285−299.
24. Polverini, E., Boggs, J. M., Bates, I. R., Harauz, G., and Cavatorta, P. (2004) Electron paramagnetic resonance spectroscopy and molecular modelling of the interaction of myelin basic protein (MBP) with calmodulin (CaM)-diversity and conformational adaptability of MBP CaM-targets, *J. Struct. Biol. 148*, 353−369.
25. Bates, I. R., and Harauz, G. (2003) Molecular dynamics exposes α-helices in myelin basic protein, *J. Mol. Model. 9*, 290−297.
26. Bates, I. R., Boggs, J. M., Feix, J. B., and Harauz, G. (2003) Membrane-anchoring and charge effects in the interaction of myelin basic protein with lipid bilayers studied by site-directed spin labeling, *J. Biol. Chem. 278*, 29041−29047.
27. Martenson, R. E. (1992) Myelin basic protein isoforms: Structural and evolutionary implications of alternative exon splicing, in *Myelin, Biology and Chemistry*, pp 387−411, CRC Press, Boca Raton.
28. Cheifetz, S., Moscarello, M. A., and Deber, C. M. (1984) NMR investigation of the charge isomers of bovine myelin basic protein, *Arch. Biochem. Biophys. 233*, 151−160.
29. Koshy, K. M., and Boggs, J. M. (1993) Interference of carbohydrates in the quantitation of protein-bound citrulline by amino acid analysis, *Anal. Biochem. 208*, 375−381.
30. Nye, S. H., Pelfrey, C. M., Burkwit, J. J., Voskuhl, R. R., Lenardo, M. J., and Mueller, J. P. (1995) Purification of immunologically active recombinant 21.5 kDa isoform of human myelin basic protein, *Mol. Immunol. 14/15*, 1131−1141.
31. Boggs, J. M., Samji, N., Moscarello, M. A., Hashim, G. A., and Day, E. D. (1983) Immune lysis of reconstituted myelin basic protein−lipid vesicles and myelin vesicles, *J. Immunol. 130*, 1687−1694.
32. Kouyama, T. K. and Mihashi, K. (1981) Fluorimetry study of N-(1-pyrenyl)iodoacetamide-labelled F-actin. Local structural change of actin protomer both on polymerization and on binding of heavy meromyosin, *Eur. J. Biochem. 114*, 33−38.
33. Kaufmann, S., Kas, J., Goldmann, W. H., Sackmann, E., and Isenberg, G. (1992*)* Talin anchors and nucleates actin filaments at lipid membranes. A direct demonstration, *FEBS Lett. 314*, 203−205.
34. Bradford, M. M. (1976) A rapid and sensitive method for the quantitation of microgram quantities of protein utilizing the principle of protein-dye binding, *Anal. Biochem. 72*, 248−254.
35. Vergères G., Manenti S., Weber T., and Sturzinger C. (1995) The myristoyl moiety of myristoylated alanine-rich C kinase substrate (MARCKS) and MARCKS-related protein is embedded in the membrane, *J. Biol. Chem. 270*, 19879−19887.
36. Gordon, D. J., Boyer, J. L., and Korn, E. D. (1977) Comparative biochemistry of non-muscle actins, *J. Biol. Chem. 252*, 8300−8309.
37. Alexander, M., and Hallett, F. R. (1999) Small angle light scattering: instrumental design and application to particle sizing, *Appl. Opt. 38*, 4158−4163.
38. Yarmola E. G., Edison A. S., Lenox R. H., and Bubb M. R. (2001) Actin filament cross-linking by MARCKS: characterization of two actin-binding sites within the phosphorylation site domain, *J. Biol. Chem. 276*, 22351−22358.
39. Peterson, G. L. (1977) A simplification of the protein assay method of Lowry et al. which is more generally applicable, *Anal. Biochem. 83*, 346−356.
40. Moscarello, M. A., Pang, H., Pace-Asciak, C. R., and Wood, D. D. (1992) The N terminus of human myelin basic protein consists of C2, C4, C6, and C8 alkyl carboxylic acids, *J. Biol. Chem. 267*, 9779−9782.
41. Eylar, E. H., Brostoff, S., Hashim, G., Caccam, J., and Burnet, P. (1971) Basic A1 protein of the myelin membrane. The complete amino acid sequence, *J. Biol. Chem. 246*, 5770−5784.
42. Hill, C. M. D., and Harauz, G. (2005) Charge effects modulate actin assembly by classic myelin basic protein isoforms, *Biochem. Biophys. Res. Commun.*, in press.
43. Grant, N. J., Aimar, C., and Oriol-Audit, C. (1983) Supramolecular forms of actin induced by polyamines; an electron microscopic study, *Eur. J. Cell Biol. 30*, 67−73.
44. Grazi, E., Magri, E., and Pasquali-Ronchetti, J. (1982) Multiple supramolecular structures formed by interaction of actin with protamine, *Biochem. J. 205*, 31−37.
45. Tang, J. X., Szymanski, P. T., Janmey, P. A., and Tao, T. (1997) Electrostatic effects of smooth muscle calponin on actin assembly, *Eur. J. Biochem. 247*, 432−440.
46. Beall, B., and Chalovich, J. M. (2001) Fesselin, a synaptopodin-like protein, stimulates actin nucleation and polymerization, *Biochemistry 40*, 14252−14259.
47. Wohnsland, F., Schmitz, A. A. P., Steinmetz, M. O., Aebi, U., and Vergères, G. (2000) Interaction between actin and the effector peptide of MARCKS-related protein. Identification of functional amino acid segments, *J. Biol. Chem. 275*, 20873−20879.
48. Tang, J. X., Janmey P. A. (1996) The polyelectrolyte nature of F-actin and the mechanism of actin bundle formation, *J. Biol. Chem. 271*, 8556−8563.
49. Libich, D. S., Hill, C. M. D., Haines, J. D., and Harauz, G. (2003) Myelin basic protein has multiple calmodulin-binding sites, *Biochem. Biophys. Res. Commun. 308*, 313−319.
50. Murray, D., Arbuzova, A., Hangyas-Mihalyne, G., Gambhir, A., Ben-Tal, N., Honig, B., and McLaughlin, S. (1999) Electrostatic properties of membranes containing acidic lipids and adsorbed basic peptides: theory and experiment, *Biophys. J. 77*, 3176−3188.
51. Uversky, V. N. (2002) Natively unfolded proteins: a point where biology waits for physics, *Protein Sci. 11*, 739−756.
52. Dyson, H. J. and Wright, P. E. (2002) Coupling of folding and binding for unstructured proteins, *Curr. Opin. Struct. Biol. 12*, 54−60.
53. Hill, C. M., Bates, I. R., White, G. F., Hallett, F. R., and Harauz, G. (2002) Effects of the osmolyte trimethylamine-N-oxide on conformation, self-association, and two-dimensional crystallization of myelin basic protein, *J. Struct. Biol. 139*, 13−26.
54. Harauz, G., Ishiyama, N., Hill, C. M., Bates, I. R., Libich, D. S., and Fares, C. (2004) Myelin basic protein-diverse conformational states of an intrinsically unstructured protein and its roles in myelin assembly and multiple sclerosis, *Micron 35*, 503−542.
55. Hartwig, J. H., Thelen, M., Rosen, A., Janmey, P. A., Nairn, A. C., and Aderem, A. (1992) MARCKS is an actin filament crosslinking protein regulated by protein kinase C and calcium-calmodulin, *Nature 356*, 618−622.
56. Wohnsland, F., Steinmetz, M. O., Aebi, U., and Vergères, G. (2000) MARCKS-related protein binds to actin without significantly affecting actin polymerization or network structure. Myristoylated alanine-rich C kinase substrate, *J. Struct. Biol. 131*, 217−224.
57. Jones, L. S., Yazzie, B., and Middaugh, C. R. (2004) Polyanions and the proteome, *Mol. Cell. Proteomics 3*, 746−769.
58. Modesti, N. M., and Barra, H. S. (1986) The interaction of myelin basic protein with tubulin and the inhibition of tubulin carboxypeptidase activity, *Biochem. Biophys. Res. Commun. 136***,** 482−489.
59. Pedraza, L. (1997) Nuclear transport of myelin basic protein, *J. Neurosci. Res. 50*, 258−264.
60. Wilson, R., and Brophy, P. J. (1989) Role for the oligodendrocyte cytoskeleton in myelination, *J. Neurosci. Res. 22*, 439−448.
61. Dyer, C. A., Philibotte, T. M., Billings-Gagliardi, S., and Wolf, M. K. (1995*)* Cytoskeleton in myelin-basic-protein-deficient shiverer oligodendrocytes, *Dev. Neurosci. 17*, 53−62.
62. Ayscough, K. R. and Drubin, D.G. (1996) ACTIN: general principles from studies in yeast, *Annu. Rev. Cell Dev. Biol. 12*, 129−160.
63. Boggs, J. M., and Rangaraj, G. (2004) Effect of phosphorylation of myelin basic protein on its interaction with actin *in vitro*, *J. Neurochem. 90* (Suppl. 1), 73.

BI0473760